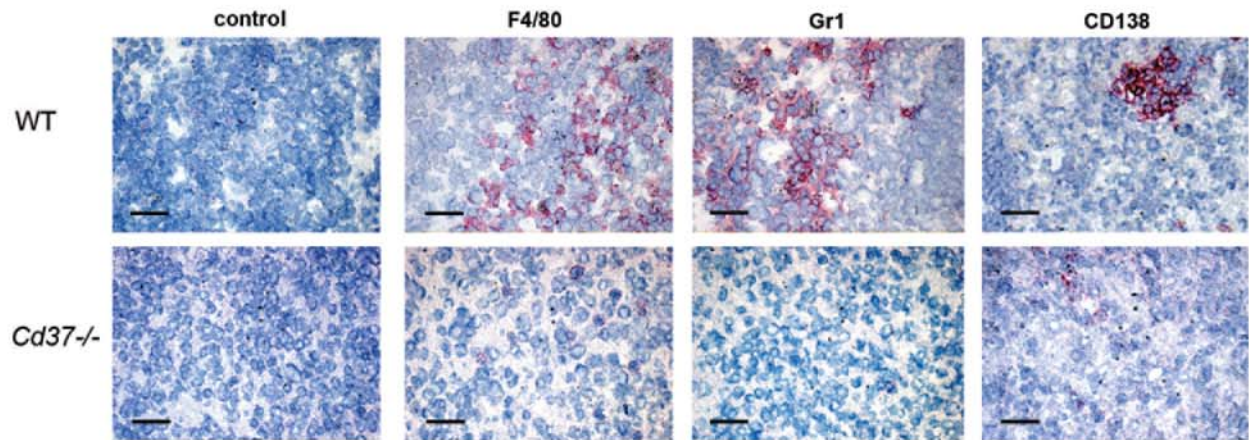
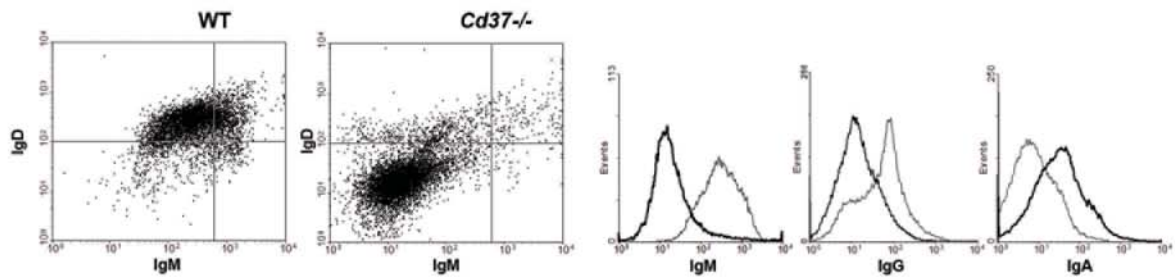


Figure S1

A



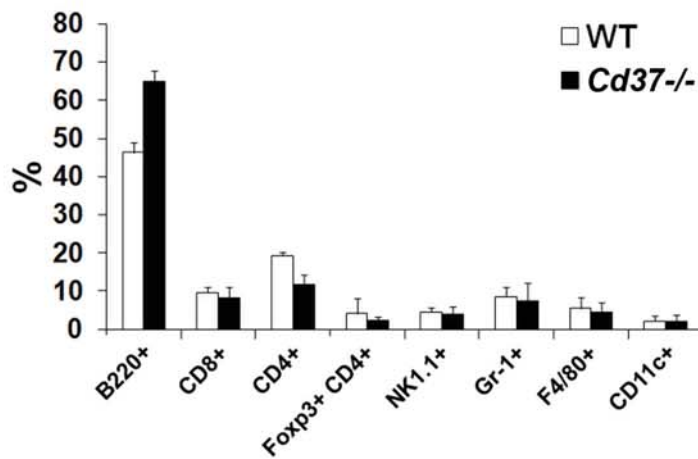
B



Supplemental Figure 1. Characterization of F4/80, Gr1, CD138, and B cell receptor expression.

(A) Immunohistochemical analyses of mLN from 18-month old WT (upper) and *Cd37*^{-/-} (lower) mice (n=4). Tissues were stained for, F4/80, Gr1 or CD138, or isotype control (data shown for rat IgG2a) using Fast-red and Hematoxylin counterstaining. Scale bars are 25 μ m. **(B)** Flow cytometry analysis of the B cell receptor (immunoglobulin) isotype on B cells from mLN of 18-month old WT (thin line) and *Cd37*^{-/-} (thick line) mice. CD19+B220+ cells were stained for IgM (x-axis, left histogram), IgD (y-axis), IgG (middle histogram) and IgA (left histogram). Experiments were performed 4 times with at least 4 mice of each genotype per group.

Figure S2

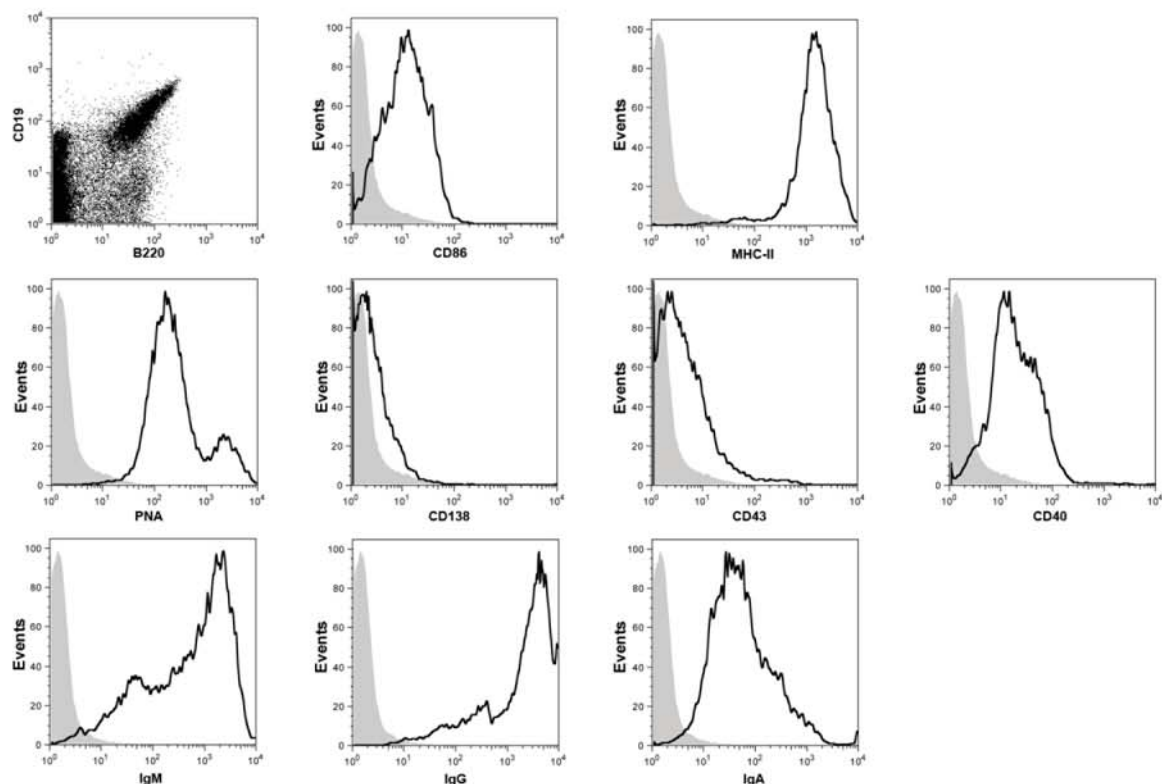


Supplemental Figure 2. Percentage of leukocyte subsets in *Cd37*^{-/-} tumors.

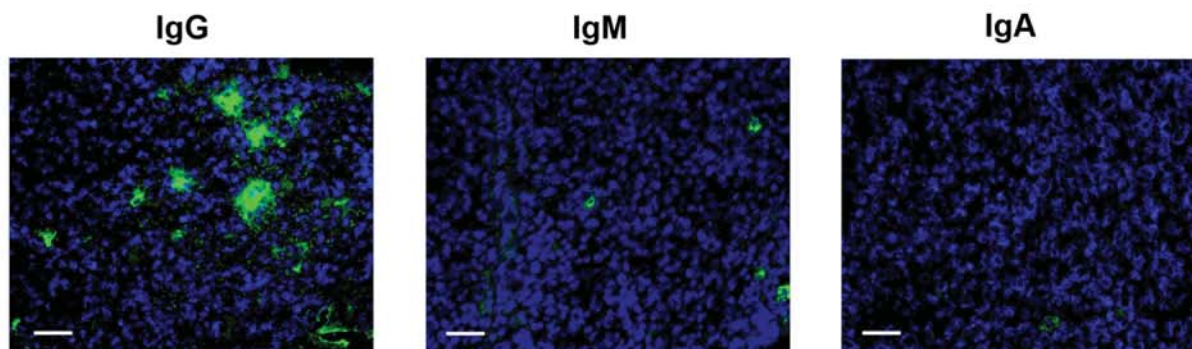
Flow cytometric analyses of leukocyte subsets in mLN from 18-month old WT (white bars) and *Cd37*^{-/-} (black bars) mice (n=6). Data show percentages of B cells (B220⁺), CD8⁺ T cells, CD4⁺ T cells, regulatory T cells (Foxp3⁺ CD4⁺), NK cells (NK1.1), granulocytes (Gr1⁺), macrophages (F4/80⁺) and dendritic cells (CD11c⁺).

Figure S3

A



B



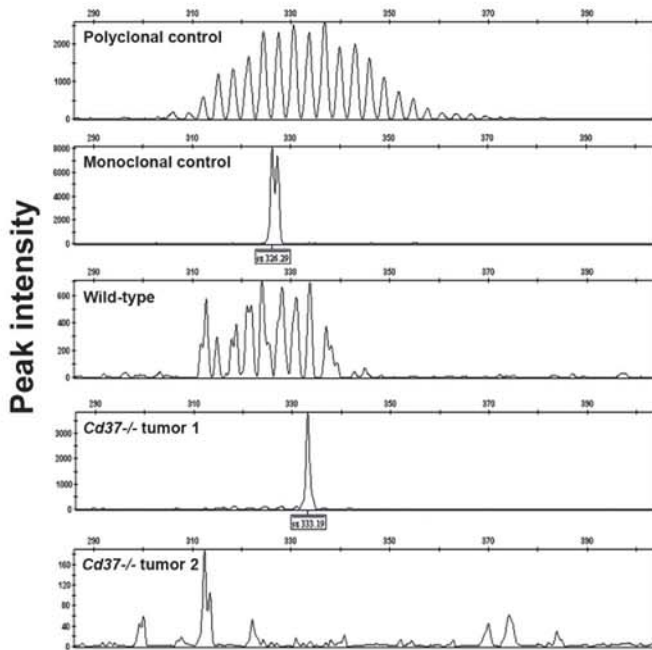
Supplemental Figure 3. Phenotypic characterization of mLN of aged tumor-bearing WT mice.

(A) B cells from mLN of 22-month old tumor-bearing WT mice were identified by gating on CD19+B220+ cells that were stained for CD86, MHC-II, PNA, CD138, CD43, CD40, IgM, IgG and IgA (black line) versus isotype control (solid grey) using flow cytometry. (B) Characterization of the B cell receptor (immunoglobulin) isotype on mLN of 22-month old tumor-bearing WT mice. Tissues were stained for IgG, IgM and IgA (green) using immunofluorescence. Nuclear counterstaining was performed with DAPI (blue). Scale bars are 70µm. Experiments were performed with tumors of 2 different WT mice yielding similar results.

Figure S4

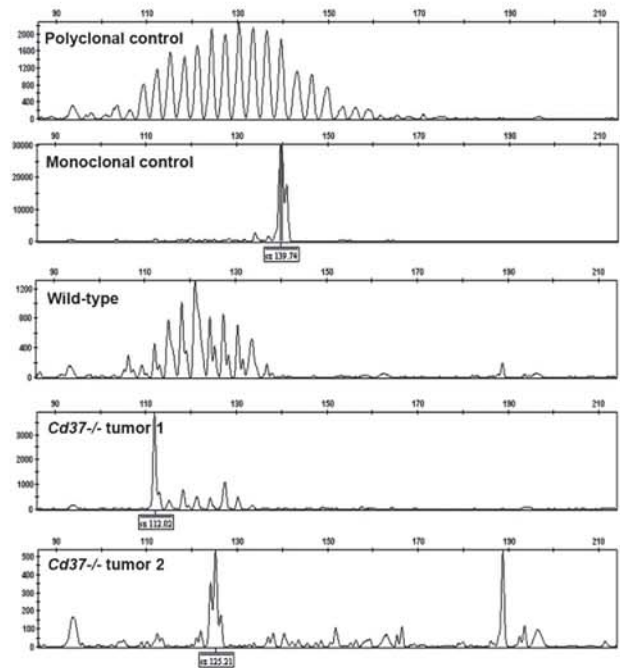
A

Fragment size (base pairs)



B

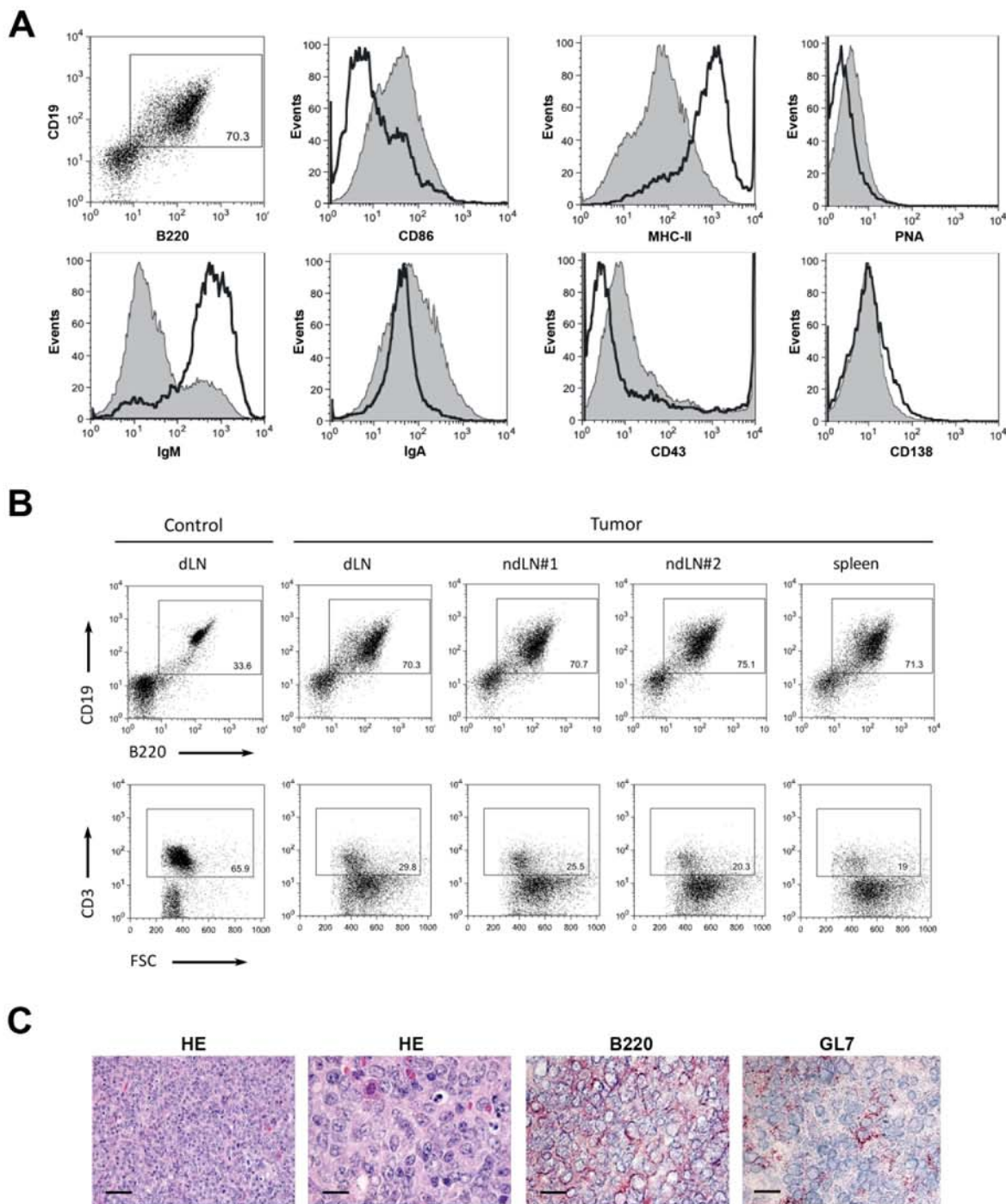
Fragment size (base pairs)



Supplemental Figure 4. Immunoglobulin clonality assessment of lymphoma tissues.

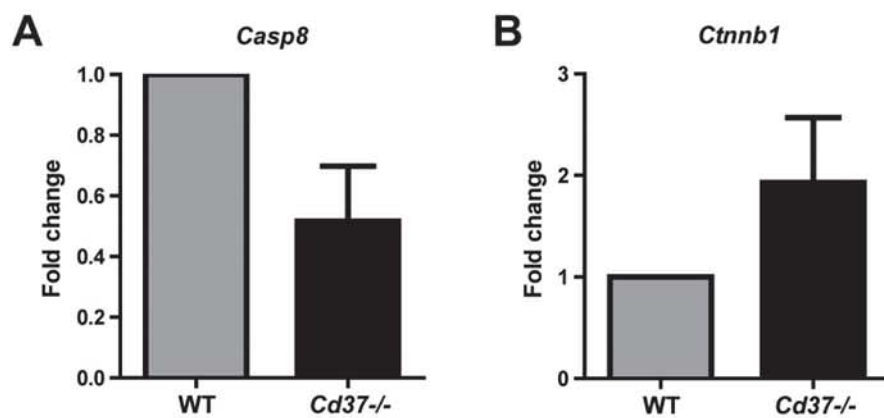
DNA was extracted from mLN of 18-month old WT and *Cd37*^{-/-} mice. VJ joinings from Ig heavy chain genes were amplified by the BIOMED-2 multiplex PCRs for IGH-VJ rearrangements, showing FR1 (A) and FR3 (B) (FR2 is shown in Figure 3A). In *Cd37*^{-/-} lymphoma tissue 2 one dominant peak in background signal was detected in FR1 and FR2, while in FR3 two dominant peaks in background signal were detected. Both FR results are consistent with monoclonality with potential presence of bi-allelic IGH rearrangements as indicated by the GeneScan pattern in FR3. Experiments were performed 2 times with 3 mice of each genotype. Data shown for two lymphomas and one WT control tissue, as well as human polyclonal and monoclonal control samples.

Figure S5



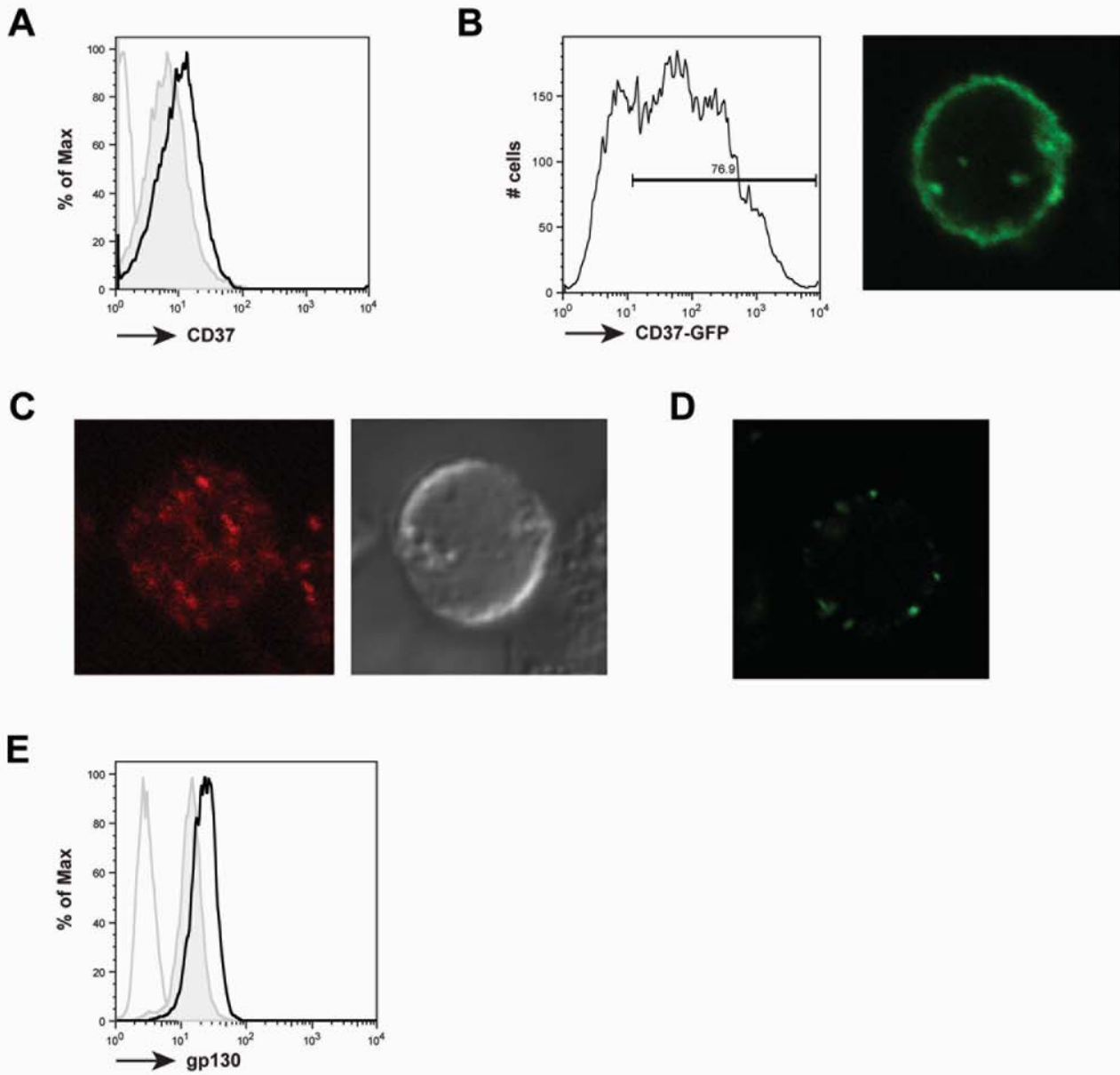
Supplemental Figure 5. Flow cytometric analyses and immunohistochemistry of tumor cells after adoptive transfer. (A) B cells were identified by gating on CD19+B220+ cells that were stained for CD86, MHC-II, PNA, CD138, CD43 and immunoglobulin receptors (IgM and IgA). Black line = WT B cells, solid grey = *Cd37*^{-/-} B cells. (B) Flow cytometry analyses of in vivo transferred lymphoma cells in different organs (draining lymph node (dLN), non-draining lymph node (ndLN), and spleen) of 6-8 weeks old *Cd37*^{-/-} mice using B220, CD19, and CD3 staining. Lymph nodes of mice that did not receive adoptively transferred lymphoma cells served as controls. Note the high percentage (70-75%) of CD19+B220+ lymphoma cells in the different lymphoid organs of mice that received the adoptive transfer indicating in vivo metastases. (C) Histology (H&E staining) and immunohistochemistry (B220 and GL7 antibodies) revealed the in vivo transferred lymphomas to be of GC-derived origin similar to the parental tumor. Scale bars are 160, 40, 40, 40 μ m (from left to right). Experiments were performed 3 times with at least 6 mice per group.

Figure S6



Supplemental Figure 6. Expression of *Casp8* and *Ctnnb1* in *Cd37*^{-/-} lymphoma cells. qPCR analysis of *Casp8* (A) and *Ctnnb1* (B) mRNA levels in WT control and *Cd37*^{-/-} tumor cells. Ct values of the genes of interest were corrected for Ct value of the housekeeping gene *Pbgd*. Fold change of *Cd37*^{-/-} mRNA levels (n≥5) were normalized to WT mRNA levels which were set at 1. Data represent mean±SEM.

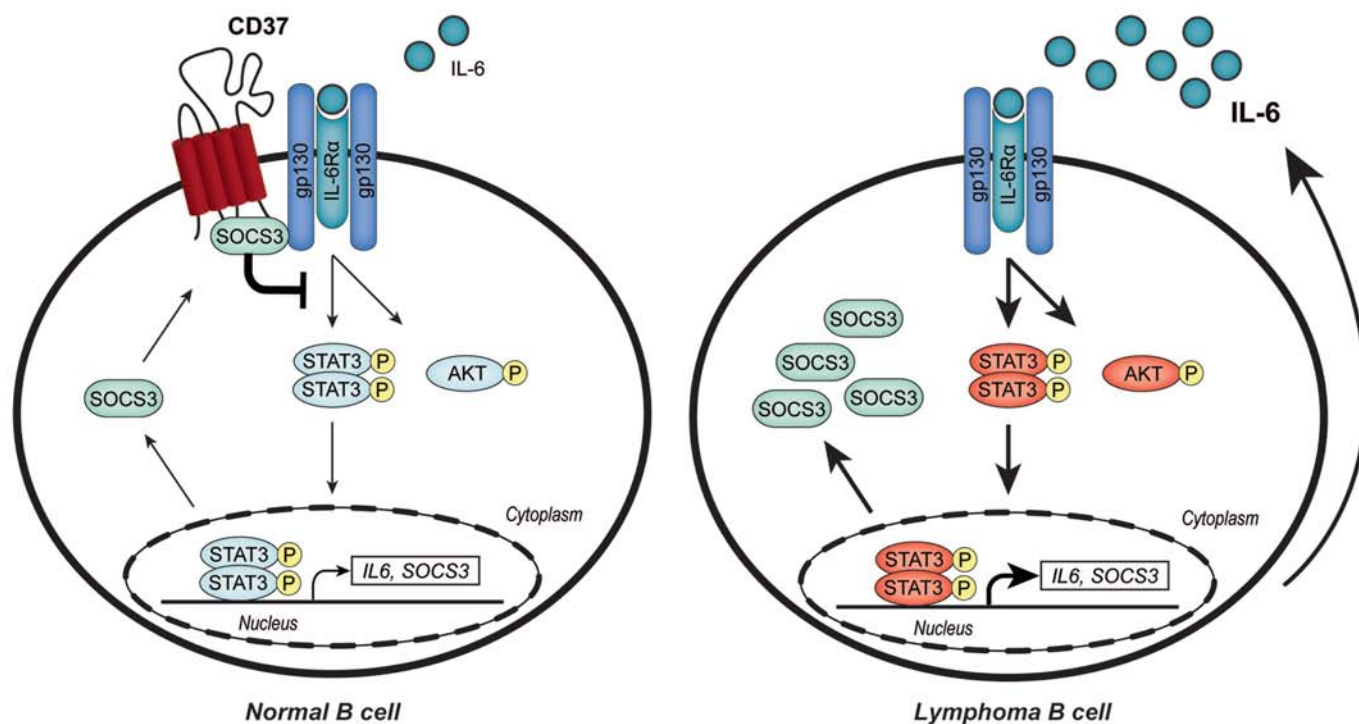
Figure S7



Supplemental Figure 7. CD37 and IL-6R expression on human NALM-6 pre-B cells.

(A) Endogenous CD37 expression on NALM-6 cells was determined by flow cytometry. Black line = CD37, solid grey = isotype control, grey line = unstained cells. (B) NALM-6 cells were transiently transfected with CD37-GFP. Transfection efficiency (= GFP expression) was determined by flow cytometry (left panel) and immunofluorescence showed membrane expression of CD37-GFP (right panel). (C-D) Endogenous intracellular SOCS3 expression (C) and surface expression of IL-6Rα (D) was determined by immunofluorescence. (E) Endogenous gp130 expression on NALM-6 cells was determined by flow cytometry. Black line = gp130, solid grey = isotype control, grey line = unstained cells.

Figure S8



Supplemental Figure 8. Model representing the function of tetraspanin CD37 in putting the brake on the IL-6 signaling pathway. In normal B cells, binding of IL-6 to the IL-6 receptor complex, consisting of IL-6R α and two gp130 chains, leads to phosphorylation of AKT and STAT3. This leads to short-term activating signals, including feed-forward production of IL-6, and long-term feedback inhibition by production of SOCS3. Once produced, SOCS3 translocates from the cytoplasm to the plasma membrane, where SOCS3 binds to both CD37 and the IL-6R complex and by this means inhibits the IL-6 signaling pathway. In *Cd37*^{-/-} lymphoma cells, SOCS3 is produced but is not able to bind to the IL-6 receptor complex due to absence of CD37. Due to autocrine production of IL-6, the IL-6 signaling pathway is constitutively active leading to accumulation of p-AKT and p-STAT3 and lymphoma cell survival.

Supplemental tables

Supplemental Table 1.

		<i>Cd37</i>^{+/+} (WT)	<i>Cd37</i>^{-/-}	<i>Cd37</i>^{-/-}<i>xIl6</i>^{-/-}
Number of mice		52	48	26
Age in months (range)		18-23	18-23	10-20
Gender	Male	27	27	13
	Female	25	21	13
Neoplasms	MLN	1	13	1
	Spleen	3	8	0
	Liver	4	10	0
Cumulative incidence (18-23 months)		8/52 (15%)	21/48 (44%)	1/26 (4%)

Supplemental Table 1. Incidence of B cell lymphomas in aged *Cd37*^{+/+}, *Cd37*^{-/-} and *Cd37*^{-/-}*xIl6*^{-/-} mice.

Supplemental Table 2.

Gene	Ct <i>Cd37</i> ^{-/-}	Δ Ct <i>Cd37</i> ^{-/-}	Ct WT	Δ Ct WT	$\Delta\Delta$ Ct	Fold change
<i>Cdkn2a</i>	32.05	4.56	34.48	7.82	-3.26	9.59
<i>Xrcc1</i>	30.12	2.63	30.89	4.23	-1.60	3.04
<i>Akt1</i>	29.65	2.16	30.27	3.61	-1.45	2.74
<i>Cdkn1a</i>	31.69	4.20	31.99	5.33	-1.13	2.19
<i>Cttnb1</i>	28.66	1.17	28.92	2.26	-1.09	2.13
<i>Jun</i>	32.38	4.89	32.55	5.89	-1.00	2.00
<i>Stat3</i>	35.42	7.93	35.58	8.92	-0.99	1.99
<i>Bax</i>	36.13	8.64	36.17	9.51	-0.87	1.83
<i>Nf2</i>	33.50	6.01	33.51	6.85	-0.84	1.79
<i>Myb</i>	32.28	4.79	32.24	5.58	-0.79	1.73
<i>Egf</i>	35.91	8.42	35.80	9.14	-0.72	1.65
<i>Trp53</i>	30.19	2.70	30.06	3.40	-0.70	1.63
<i>Tnf</i>	35.69	8.20	35.49	8.83	-0.63	1.55
<i>S100a4</i>	30.12	2.63	29.82	3.16	-0.53	1.45
<i>Fos</i>	34.52	7.03	34.13	7.47	-0.44	1.36
<i>Atm</i>	31.01	3.52	30.59	3.93	-0.41	1.33
<i>E2f1</i>	33.78	6.29	33.32	6.66	-0.37	1.29
<i>Nfkbia</i>	27.89	0.40	27.34	0.68	-0.28	1.22
<i>Cdk4</i>	30.76	3.27	30.16	3.50	-0.23	1.17
<i>Brca2</i>	34.02	6.53	33.39	6.73	-0.20	1.15
<i>Mlh1</i>	30.43	2.94	29.72	3.06	-0.12	1.09
<i>Mgmt</i>	33.46	5.97	32.74	6.08	-0.11	1.08
<i>Wwox</i>	35.85	8.36	35.09	8.43	-0.07	1.05
<i>Ets1</i>	31.99	4.50	31.21	4.55	-0.05	1.04
<i>Men1</i>	35.11	7.62	34.31	7.65	-0.03	1.02
<i>Hras1</i>	31.21	3.72	30.41	3.75	-0.03	1.02
<i>Tgfb1</i>	29.67	2.18	28.86	2.20	-0.02	1.02
<i>Kitl</i>	32.55	5.06	31.72	5.06	-0.00	1.00
<i>Igf2r</i>	32.79	5.30	31.95	5.29	0.01	0.99
<i>Pik3c2a</i>	32.99	5.50	32.13	5.47	0.03	0.98
<i>Elk1</i>	36.34	8.85	35.47	8.81	0.04	0.97
<i>Mdm2</i>	30.45	2.96	29.55	2.89	0.07	0.95
<i>Esr1</i>	36.25	8.76	35.32	8.66	0.10	0.93
<i>Raf1</i>	30.53	3.04	29.6	2.94	0.10	0.93
<i>Stk11</i>	30.57	3.08	29.61	2.95	0.13	0.92
<i>Bcl2l1</i>	36.34	8.85	35.32	8.66	0.19	0.88
<i>Src</i>	34.69	7.20	33.6	6.94	0.26	0.84
<i>Nras</i>	31.36	3.87	30.26	3.60	0.27	0.83
<i>Nf1</i>	35.89	8.40	34.76	8.10	0.30	0.81
<i>Cdh1</i>	34.94	7.45	33.79	7.13	0.32	0.80
<i>Cdkn2b</i>	33.73	6.24	32.54	5.88	0.36	0.78
<i>Sh3pxd2a</i>	31.61	4.12	30.36	3.70	0.42	0.75
<i>Hgf</i>	34.25	6.76	32.95	6.29	0.47	0.72
<i>Bcr</i>	36.29	8.80	34.98	8.32	0.48	0.72
<i>Rara</i>	32.62	5.13	31.26	4.60	0.53	0.69
<i>Nfkb1</i>	31.50	4.01	30.14	3.48	0.53	0.69
<i>Rel</i>	32.20	4.71	30.84	4.18	0.53	0.69
<i>Mcl1</i>	29.65	2.16	28.28	1.62	0.54	0.69
<i>Pik3ca</i>	32.87	5.38	31.48	4.82	0.56	0.68
<i>Runx3</i>	32.74	5.25	31.32	4.66	0.59	0.67
<i>Brca1</i>	34.58	7.09	33.14	6.48	0.61	0.66
<i>Kras</i>	31.68	4.19	30.14	3.48	0.71	0.61
<i>Rb1</i>	33.34	5.85	31.78	5.12	0.73	0.60
<i>Vhl</i>	30.45	2.96	28.87	2.21	0.75	0.60
<i>Apc</i>	33.34	5.85	31.74	5.08	0.77	0.59
<i>Kit</i>	33.34	5.85	31.72	5.06	0.79	0.58
<i>Prkca</i>	32.26	4.77	30.61	3.95	0.82	0.57
<i>Zhx2</i>	33.06	5.57	31.33	4.67	0.90	0.54
<i>Ccnd1</i>	33.00	5.51	31.21	4.55	0.96	0.51
<i>Myc</i>	32.51	5.02	30.60	3.94	1.08	0.47
<i>Smad4</i>	31.65	4.16	29.68	3.02	1.14	0.45
<i>Runx1</i>	31.72	4.23	29.74	3.08	1.15	0.45
<i>Rassf1</i>	32.54	5.05	30.48	3.82	1.23	0.43
<i>Bcl2</i>	32.76	5.27	30.23	3.57	1.70	0.31
<i>Casp8</i>	35.17	7.68	32.42	5.76	1.92	0.26
<i>Jak2</i>	34.45	6.96	31.12	4.46	2.50	0.18

Supplemental Table 2. Molecular signature of oncogenes and tumor suppressor genes in *Cd37*^{-/-} lymphomas. Cancer gene profiling approach by performing an Oncogenes and Tumor suppressor genes Array on mLN from WT mice and lymphoma-bearing *Cd37*^{-/-} mice (aged-matched). Δ Ct values are corrected for mean Ct value of five housekeeping genes (*Gusb*, *Hprt1*, *Hsp90ab1*, *Gapdh*, *Actb*).